https://doi.org/10.1016/j.jclepro.2020.123407

Wordcount :7807 words

Optimization strategies and verifications of negative thermal-flux region occurring in parabolic trough solar receiver

Qiliang Wang [1, 2], Honglun Yang [2], Mingke Hu [3], Jingyu Cao [2], Gang Pei [2, *], Hongxing Yang [1]

[1] *Renewable Energy Research Group (RERG), Department of Building Services Engineering, The Hong Kong Polytechnic University, Hong Kong, China*

[2] *Department of Thermal Science and Energy Engineering, University of Science and Technology of China, Hefei 230027, China*

[3] *Institute of Sustainable Energy Technology, University of Nottingham, University Park, Nottingham NG7 2RD, UK*

* Corresponding author. Tel.: +86 551-63601652. E-mail address: peigang@ustc.edu.cn

Abstract

Prospects for parabolic trough collector are growing as the market increasingly values concentrated solar-thermal utilization. Parabolic trough solar receivers, the key components of parabolic trough collector system, seriously suffer degradation of photothermal conversion performance at high operating temperature due to considerable emissive heat loss, which exerts significantly negative influence on the overall performance and development of parabolic trough collector and subsequent thermal utilization systems. This study examines the spectral emissive heat loss and circumferential heat transfer characteristics around the parabolic trough solar receiver. In this framework, a new concept is proposed, i.e. the negative thermal-flux region in which negative net heat gain occurs, accordingly enlightening and giving birth to new optimization strategies for reducing emissive heat loss of the parabolic trough receiver. A novel parabolic trough receiver with an inner radiation shield in the negative thermal-flux region is designed, manufactured and comprehensively tested.

The results show a validity of the existence of the negative thermal-flux region and great potential of new optimization methods to achieve breakthrough enhancement of heat-collecting performance in parabolic trough collector system. Compared with the prototype solar receiver, the heat loss of proposed solar receiver is effectively reduced by 28.1% at absorber temperature of 600 °C, the heat-collecting and exergetic efficiencies are significantly enhanced by 12.9 and 17.6 % at the solar irradiance of 600 W/m^2 and inlet temperature of 550 °C.

KEYWORDS: *Parabolic trough collector; Solar receiver; Photothermal conversion; Heat loss; Efficiency*

Nomenclature

a	Ambient
f	fluid
g	Glass envelop
h	Convection heat transfer coefficient, W/(K·m^2)
k	Radiation shield
r	radiated
s	Absorber tube
A	Area, m^2
A'	Unit area, m
E	Blackbody's emissive power, W/m^2
F	View factor
G	Direct solar irradiance, W/m^2
J	Radiosity, W/m^2
L	Length, m
P	Electrical power, W
in	Inlet
ou	Outlet

Abbreviation and subscripts

PTC	Parabolic trough collector
CSP	Concentrated solar power
PTR	Parabolic trough receiver
HTF	Heat transfer fluid
SSC	Solar selective-absorbing coating
NTR	Negative thermal-flux region
RS	Radiation shield
HL	Heat loss, W/m
PTR-RS	PTR with a RS
RMSD	Root-mean-square deviation
RP	Relative percentage, %

Greek Symbols

η	Efficiency

Q	Net heat flux, W/m^2	θ	Angle, °
R	Thermal resistance, 1/m	γ	Thermal flux ratio
T	Temperature, K	ε	Emittance
abs	Absorbed	α	Absorptance
ap	Aperture	τ	Transmittance
conv	Convective	λ	Wavelength, μm
emi	emitted		

1. Introduction

Accessibility of solar energy to obtain high-temperature heat source is accomplished mainly by concentrated solar-thermal technologies (Li, 2019; Pitz-Paal, 2017; Li et al., 2020). Of them, parabolic trough collector (PTC) is a pretty proven and promising technology (Fernández-García, 2015). In PTC systems, direct solar irradiance projects on the parabolic trough mirrors which have high specular reflectance and then is reflected to parabolic trough solar receiver (PTR) placed along focal line of parabolic trough mirrors (Fuqiang et al., 2017; Li et al., 2020). As the core components and major occurring sites of photothermal conversion process in PTC system, PTRs are popularly designed for maximizing the absorption to the solar irradiance besides of adequate quality reliability in commercial. With high transmittance of glass envelope and covering of solar selective-absorbing coating (SSC) on the absorber tube in PTR (Wang et al., 2019), PTR absorbs 90~93% of normal direct solar irradiance which is then converted into and stored as the heat energy of heat transfer fluid (HTF) flowing inside of PTR (Bellos and Tzivanidis, 2019). Eventually, the heat energy of HTF is transferred and applied to the rear terminal systems with many varieties such as electrical power generation system (Mahlangu and Thopil, 2018; Khan and Arsalan, 2016; He et al., 2020), heating or cooling supply systems (Chen et al., 2019; Trieb et al., 2009; Koroneos and Tsarouhis, 2012).

Generally, HTF temperature achieved through PTC solar field could reach approximately 400°C and 550 °C

in commercial power plants when synthetic oil and molten salt are selected as HTF (Feldhoff et al., 2012; Maccari et al., 2015), respectively. For elevation of power generation efficiency, higher temperature heat source collected in PTR is being pursued. In the other hand, however, serious degradation of photothermal conversion performance occurs in PTR at such high operating temperature. The heat-collecting efficiency, which is used to represent photothermal conversion performance, trends to rapidly decrease with operating temperature raised to second even third power (Duffie and Beckman, 2020), which meanwhile exerts significantly negative impacts on the overall performance of rear terminal system thus limits the extended application of PTC system in the future (Zhang et al., 2013). Therefore, effective enhancement of photothermal conversion performance of PTR has urgent significance for the technical breakthrough and further development of PTC system.

Basically, high photothermal conversion performance of PTR requires high solar irradiance absorption and low emissive heat loss for PTR. To date, most researchers focus on enhancement of solar irradiance absorption of PTR by reinforcing component materials' properties or HTF heat transfer in PTR. Enhancements of solar transmittance of glass envelope (Wirz et al., 2014), solar irradiance absorptance of SSC (Cespedes et al., 2014; Soum-Glaude et al., 2017), heat transfer between HTF and absorber tube (Singh and Khullar, 2019; Dugaria et al., 2018), etc. are popular optimization approaches proposed. Actually, however, all of these optimization approaches paly limited roles in further significant improvement of solar irradiance absorption of PTR. The solar transmittance of glass envelope and absorptance of SSC have already reached 96% with the fruitful researches on material, almost approaching to the materials' optimization celling (López-Herraiz et al., 2017). The total absorption amount of PTR to solar irradiance has a handful of increase even assuming elevation of a few more percentage points of transmittance and absorptance. The heat transfer enhancement between HTF and absorber tube is generally accomplished by addition of materials with better thermal properties into HTF

or designing new structures inside of absorber tube (Cheng et al., 2012; Jaramillo et al., 2016; Bellos et al., 2020). Absolutely, these optimization methods exert a certain effectiveness, but incredibly incurring other technical or practical problems. Additionally, it is hardly possible to realize a breakthrough improvement of photothermal conversion performance of PTR only by enhancing the heat transfer characteristic of HTF, because this optimization method could not effectively reduce the heat loss from the source nor substantially increase amount of absorption of incident solar irradiance by PTR.

As the other one basic element determining photothermal conversion performance of PTR, emissive heat loss is unignored from technical and practical perspectives. According to widely recognized experimental data conducted by NREL (Burkholder and Kutscher, 2009), the emissive heat loss accounts for almost 19.4% and 26.8% of direct solar irradiance received by PTR at absorber temperature of 550 °C and 600 °C under assumption of 600 W/m^2 direct solar irradiance. This means fatal decreases by absolute proportions over 19.4% and 26.8% of heat-collecting efficiency in PTC system would occur and thus cause huge degradation of thermal performance of PTR. This phenomenon of considerable heat loss at high operating temperature can be conclusively explained by Planck's law and Wien's displacement law (Incropera et al., 2007). Here, we take Schott PTR70 solar receiver (Benidir et al., 2018) as study case. blackbody's emissive heat from absorber tube explosively grows with absorber temperature raised to fourth power according to Planck's law, accordingly, the eventual emissive heat loss increases with almost same functional relation. In addition, the whole body of blackbody's emissive heat gradually shifts to shorter wavelength according to Wien's displacement law, and partially overlaps with the solar irradiance wavelength band lower than 2.5μm (Figure 1). Though SSC on the absorber tube has low spectral emittance in infrared wavelength (approximately ＞ 2.5 μm), high spectral absorptance (spectral emittance) of SSC to solar irradiance counterproductively results in escape of a fair amount of radiation heat from PTR by overlapping band window especially at higher

operating temperature. The spectral radiation heat transfer on the surface of absorber tube exhibited in Figure 1 is calculated with high precision based on the established spectral thermal radiation model (section 3.3.1) (Wang et al., 2017). Approximately 20.2%, 31.4 %, and 42.3% of total emissive heat loss in PTR at absorber temperature of 400, 500, and 600 °C locate in the overlapping band window. Therefore, high solar absorptance of SSC in overlapping band window inadvertently contributes to the increase of heat loss.

On the basis of above insight on the spectral thermophysical characteristic of PTR, it is concluded that the massive heat loss with an exponential increase is inevitable with increasing absorber temperature if only the pursuit of high solar irradiance absorption of PTR. This phenomenon causes less effectiveness of photothermal conversion performance of PTR improvement only by enhancing solar irradiance absorption, thus, this indisputable fact of unignored emissive heat loss prompt us to reflect on the optimization direction of pursuing high solar irradiance absorption. Absolutely, reduction of emissive heat loss accomplished by new optimization methods should be the first priority to improve photothermal conversion of PTR without too much incurred loss of solar irradiance absorption.

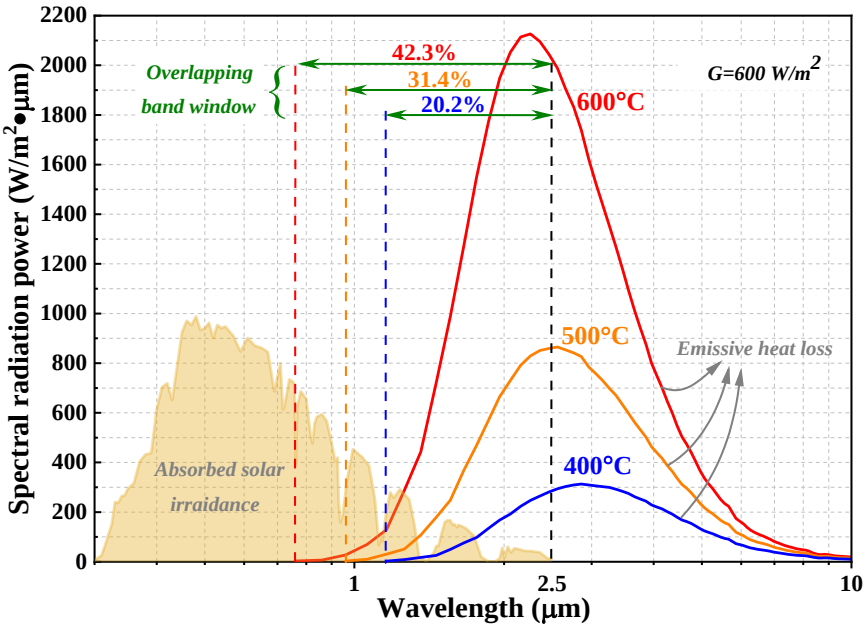

Figure 1. Spectral emissive heat loss and overlapping band window. Spectral band of emissive heat loss of PTR at high absorber temperature overlaps with that of absorbed solar irradiance, thus forming overlapping band window in which increasing

proportion of heat loss locates with higher absorber temperature.

In this paper, we examine the circumferential heat transfer characteristics around PTR integrated with the spectral emissive heat loss and spectral absorbed solar irradiance by PTR, and propose a new concept of negative thermal-flux region in which negative net heat gain appears. In this framework, four kinds of novel optimization strategies, aiming to reduce heat loss and thus improve comprehensive photothermal conversion performance in negative thermal-flux region in PTR, are put forward. Furthermore, a novel parabolic trough receiver with an inner radiation shield in the negative thermal-flux region is designed, manufactured and comprehensively tested in indoor and outdoor experiments. In addition, mathematical models of heat loss, heat-collecting efficiency and exergetic efficiency with high precision are established to observe and study the overall thermal performance of PTR with a radiation shield at higher operating temperature. The simulation results yield a good consistence with the experimental data. The results validate the efficient improvement of net heat gain in negative thermal-flux region by inserting a radiation shield, and show that the proposed optimization methods achieve great potentials for the enhancement of the photothermal conversion performance of the PTR.

2. Negative thermal-flux region and optimization strategies

Similar to the spectral radiation heat distribution as shown in Figure 1, the spectral distributions of absorbed solar irradiance and emissive heat loss at each point around the absorber tube can be accurately calculated, then we can obtain total amount of solar irradiance absorption and emissive heat loss in circumferential to investigate circumferential heat transfer characteristic of PTR. In this paper, it should be pointed out that solar irradiance absorption and emissive heat loss are represented by dimensionless parameters of thermal flux ratio γ_{abs} and γ_{emi}, which are the ratios of amount of solar irradiance absorption (Q_{abs}, W/m^2) and emissive heat loss (Q_{emi}, W/m^2) to the direct solar irradiance (G, W/m^2) for easy comparison and intuition. In this framework,

we take popularly typical EuroTrough collector (Al-Soud and Hrayshat, 2009) and Schott PTR70 as the analysis case. With determined parameters of PTC system, values of γ_{abs} around absorber tube is confirmed as depicted in Figure 2. Concentrated solar irradiance reflected by trough mirrors almost focuses on the lower part of PTR with angle θ ranging from 70 to 290°, but the upper part of PTR ranging approximately from 0 to 70° and from 290 to 360° only receives one solar irradiance, where γ_{abs} reaches maximum value of 0.94 at the top point. Different with uneven solar irradiance, the emissive heat loss is circumferentially uniform under an acceptable assumption of same temperature around absorber tube. In the case of solar irradiance of 600 W/m^2 and absorber temperature of 600 °C, γ_{emi} are 7.01 which is obviously larger than the values of γ_{abs} at the angle θ from 0 to 85° and from 275 to 360°, at which the value of γ_{emi} is 9.9 times as many as the average value of γ_{abs}, demonstrating emissive heat loss is almost 10 times solar irradiance absorbed by PTR. Apparently, the net heat gain of PTR in this part with angle of 0~85° and 275~360° is negative, thus we named this part of PTR *negative thermal-flux region* (NTR) or n*egative energy-flow region*, and the other part of PTR *nonnegative thermal-flux region* (non-NTR). The net heat gains in NTR and non-NTR are represented by the sum of difference between γ_{abs} and γ_{emi} at each angle. Detailed expressions are described as $[\int_0^{7\pi/36}(\gamma_{abs}-\gamma_{emi})+\int_{55\pi/36}^{2\pi}(\gamma_{abs}-\gamma_{emi})]$ and $\int_{7\pi/36}^{55\pi/36}(\gamma_{abs}-\gamma_{emi})$ in rad, hence the net heat gains in NTR and non-NTR are calculated as –5.95π and 39.62π rad, respectively. The total heat gain of PTR is significantly reduced by 15.0 % due to the encroachment of negative net heat gain in NTR, in other words, existence of NTR results in serious decrease of heat-collecting efficiency of PTC system by absolute 15.0 %. Even worse, the negative impacts of NTR on PTC system would further accentuated in real operating conditions with cosine loss, tracking error, cleanness of mirrors and other problems, because the net heat gain in non-NTR would be reduced by these factors and negative net heat gain in NTR will reinforce adverse impacts on the thermal performance of PTR and PTC system.

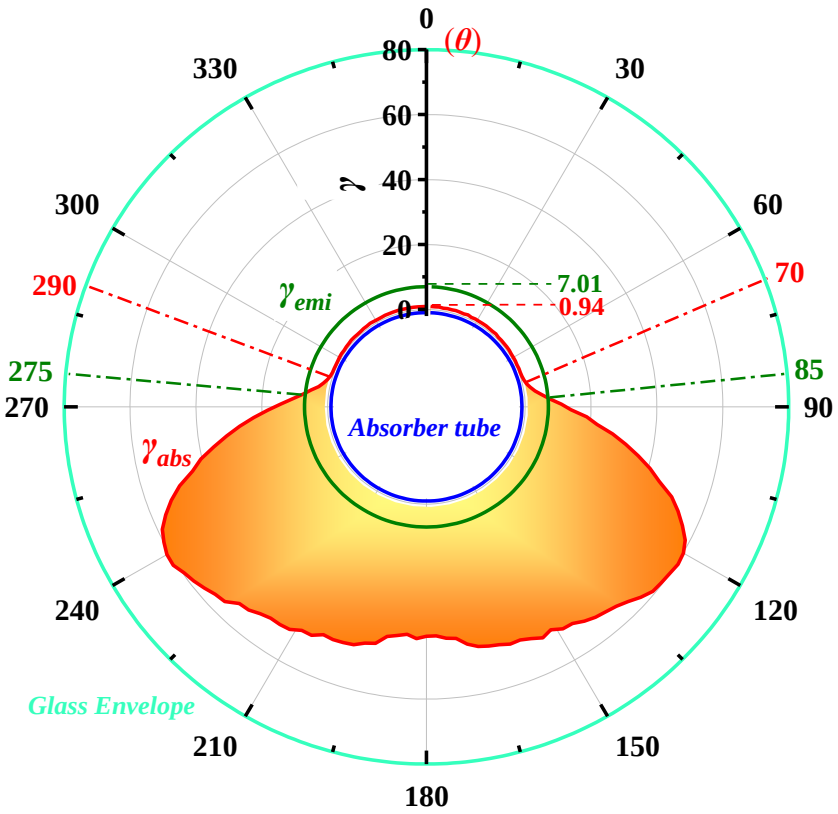

Figure 2. Circumferential solar irradiance absorption and emissive heat loss around PTR. They are calculated within high precision within 6.0% deviation. Negative thermal-flux region (NTR) in which net heat gain is negative locates in the upper part of PTR at the angle of 0~85° and 275~360° in ideal operation condition. The scope of NTR would be slightly shrunken or enlarged due to solar rays focusing accuracy problem arisen in real operating PTC system.

Discovery of NTR reveals the undetectable heat transfer characteristics occurring in PTR, and points out accessible optimization directions to enhance photothermal conversion performance of PTR, that is to improve the net heat gain in NTR by reinforcing the reduction of emissive heat loss in NTR. An important point to get access is that certain amount of solar irradiance absorption of PTR in NTR may lose as the optimization methods take heat loss reduction in NTR as the first priority, but it is acceptable if net heat gain of NTR is improved.

Here, novel optimization methods proposed based on NTR can be concluded from four aspects. Firstly, shift optimization of cutoff wavelength of SSC in NTR to short-wave for lowering emittance in overlapping band window; secondly, optimization of vacuum annular in NTR by introducing functional structures or materials

to block emissive heat loss from absorber tube; thirdly, optimization of coating materials covered on glass envelope in NTR for enhancing reflectance in overlapping band window to intercept the emissive heat loss; at last, optimization of outside space of PTR in NTR by adding functional structures for the blockage of emissive heat loss. All these methods can effectively reduce the emissive heat loss in NTR, in the meanwhile, inevitably causing a certain solar irradiance absorption loss for absorber tube in NTR.

3. Experiments, Models, and Methodology

3.1 Novel PTR with a radiation shield

In this paper, we designed, manufactured and tested a novel PTR by introducing a radiation shield (RS) into vacuum annular in NTR according to the second optimization method (Figure 3 (a)). RS in the shape of an arc is made of lightweight aluminum sheet, and inner surface towards to absorber tube is polished aluminum, the outer surface towards to glass envelope is eventually determined as solar selective-absorbing coating (SSC) after performance analysis with different coatings on RS. The angle of RS surrounding absorber tube and diameter of RS are set as 120° and 85 mm, respectively. The detailed parameters of prototype PTR (PTR) and novel PTR with RS (PTR-RS) are presented in Table 1 and Table 2.

Table 1. Specifications of the tested PTR and PTR-RS

Component	Material	Dimension
Absorber tube (PTR and PTR-RS)	stainless steel	Length: 4060 mm Outer diameter: 70 mm Thickness: 3 mm
Glass envelope (PTR and PTR-RS)	Low-iron borosilicate glass	Outer diameter: 125 mm Thickness: 2.5 mm
Radiation shield (PTR-RS)	Aluminum sheet	Diameter: 80 mm Angle: 120°

Table 2. Optical parameters of components in PTR and PTR-RS

Parameter	Value	Parameter	Value
ε_s	0.09@400°C	α_s	0.96
τ_s	0.96	$\varepsilon_{k,\ inner}$	0.04@400°C
$\varepsilon_{k,\ outer}$	0.09@400°C	$\alpha_{k,\ outer}$	0.96

Noted: k represents radiation shield in PTR-RS. ε, τ, and α refer to emittance, transmittance, and absorptance. *outer* and *inner* represent the outer surface and inner surface, respectively.

3.2 Experiments and Methodology

The indoor and outdoor experiments of PTR and PTR-RS were carried out in standard test laboratory located in Institute of Electrical Engineering (IEE), Chinese Academy of Science for observing their emissive heat losses and heat-collecting efficiencies, respectively.

Indoor heat loss tests employed energy balance method. The tested PTR and PTR-RS were heated by electric heaters inserted inside of absorber tube to achieve the desired testing absorber temperature as exhibited in Figure 3(b). The ends of the PTR and PTR-RS were wrapped with asbestos for heat insulations. In a testing process, the desired absorber temperature was determined and set in the control platform system, the current of heaters was then switched on, and the absorber tube was heated by the heaters. In the heating process, total 6 thermocouples were used to monitor the transient absorber temperature, this process was considered available when all of measured temperatures of 6 thermocouples were within the temperature differences of 10 °C at most. As a result, the emissive heat loss can be calculated out according to electric powers of heaters under quasi-static equilibrium state of testing process which lasts 20 mins. The total heat loss in the PTR or PTR-RS can be expressed as:

$$HL = \frac{P}{L}, \tag{1}$$

where, HL is the total heat loss, W/m. P is the total electric powers of the heaters, W. L is the length of PTR,

m.

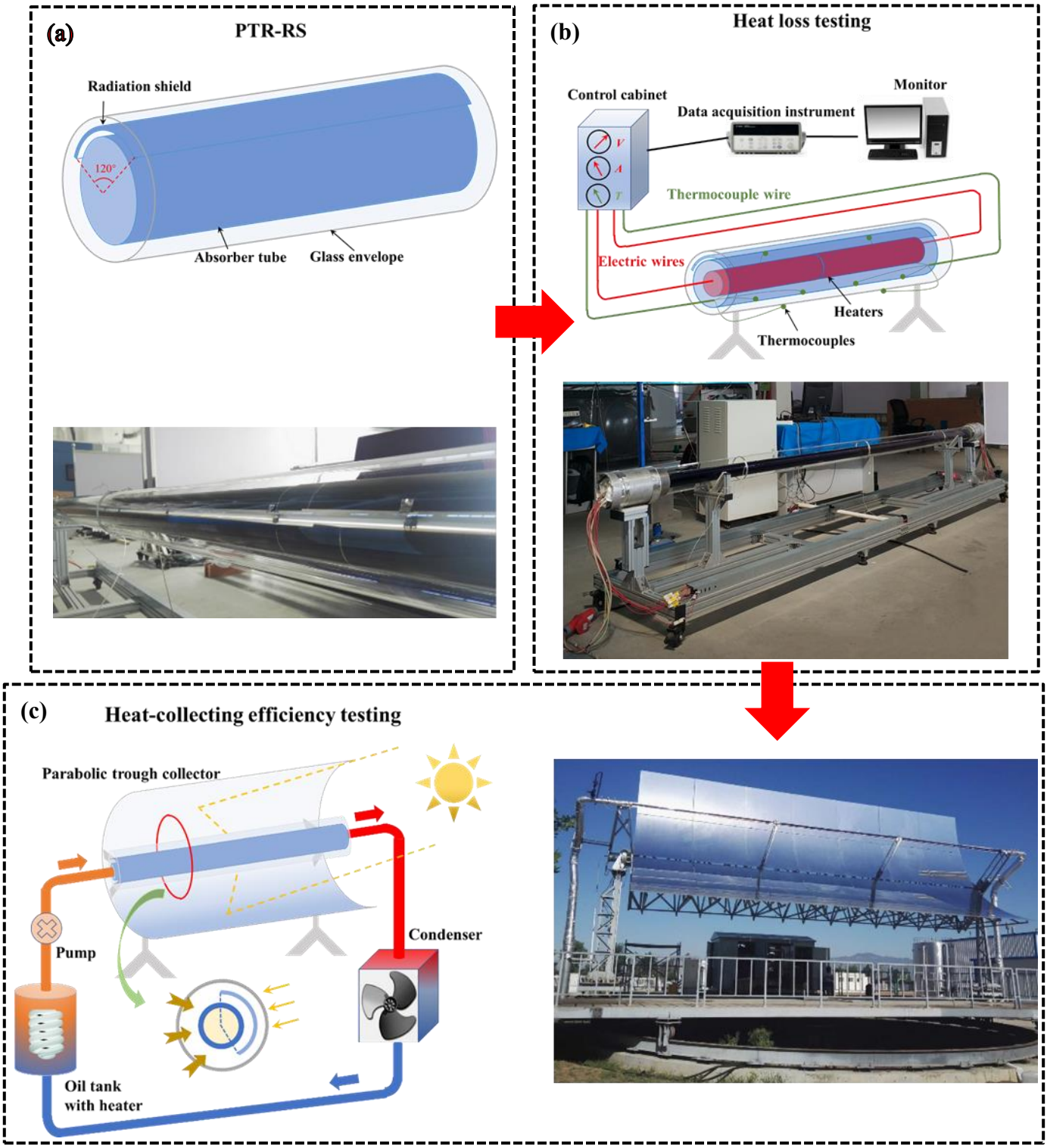

Figure 3. Schematic representation and photographs of PTR-RS and experiments. (a) PTR-RS: arc-shaped RS with angle of 120° is inserted into vacuum annular in NTR to block the emissive heat from absorber tube, which is fixed on the absorber tube by a support pillar. (b) Indoor heat loss experiment: indoor tests employed inserted electric heaters to achieve desired testing absorber temperatures, emissive heat loss is calculated out by monitored electric powers of heaters. (c) Outdoor heat-collecting efficiency

experiment: outdoor test platform employed two-axis tracking system, the heat-collecting efficiency is obtained based on the measured operating and environmental parameters under quasic-static state.

The PTC module in outdoor rotating test platform is a standard Eurotrough collector with width of 5.76 m and length of 12 m as shown in Figure 3(c). It employed two-axis tracking system, which can accurately tract the sun in a whole day within errors of 0.02° in azimuth and altitude angles. The thermocouples and flowmeters were installed in the inlet and outlet ends of the PTC testing platform to monitor the transient fluid temperatures and mass flow rate. In an experimental process, silicone oil used as HTF (Vignarooban et al., 2015) in tank was preheated or cooled to the desired inlet temperature by the control system, then flowed through the PTC platform with the tested solar receivers and returned back to tank in cycle. The testing process is regraded as a quasi-static state once monitored inlet temperature, outlet temperature, and mass flow rate fluctuate within 0.2 °C in 5 mins. Outdoor experiments were carried out under a determined volume flow rate of 15.0 m^3/h, inlet temperatures approximately from 250 °C to 360 °C.

The measured heat-collecting efficiency of the PTC (η) can be expressed as the optical efficiency (η_0) minus an efficiency penalty term ($\eta^{'}$) (Kutscher et al., 2012),

$$\eta = \eta_0 - \eta^{'}, \tag{2}$$

the value of $\eta^{'}$ in this study can be achieved by the expression as follows:

$$\eta^{'} = \frac{nHL}{A_{ap}G}, (n=3) \tag{3}$$

where, n is the number of the HCEs contained in the PTC testing platform; A_{ap} is aperture area of tested PTC module, m^2, its value is 69 m^2 in this study. G represents direct normal solar irradiance, W/m^2. It can be concluded from Equation (3), $\eta^{'}$ is mainly dependent on the variable of heat loss which is virtually proportional to absorber temperature raised to the third or fourth power, thus the value of $\eta^{'}$ would be operating temperature raised to second or third power. For fitting well to the experimental data, the abscissa of the temperature

difference divided by the G raised to a fractional power is employed to collapse various radiation curves into a single curve (Kutscher et al., 2012). For PTR studied in this paper, a nonlinear regression showed the best-fit exponent to be 0.5, thus the expression of the heat-collecting efficiency plotted versus reduced temperature ($\frac{T_f - T_a}{G^{0.5}}$) can be written as:

$$\eta = \eta_0 - A\frac{T_f - T_a}{G^{0.5}} - B(\frac{T_f - T_a}{G^{0.5}})^2, \tag{4}$$

where A and B are coefficients responding to the linear item and quadratic item, T_f and T_a represent average fluid temperature of PTC module and ambient temperature, K. T_f is expressed as follows:

$$T_f = \frac{T_{in} + T_{ou}}{2}, \tag{5}$$

where T_{in} and T_{ou} are inlet temperature and outlet temperature of heat transfer fluid in PTC module, K.

3.3 Mathematical Models

3.3.1 heat loss model

Conventional heat transfer model popularly uses average parameters in whole wavelength of components in PTR (Kalogirou, 2012), such as the average absorptance of SSC to solar irradiance, transmittance of glass envelope, etc., and then calculate the heat flux among different components in PTR by the empirical heat transfer formula. These conventional heat transfer models can play an efficient role in simulating and predicting the thermal performance of PTR at low operating temperature. However, they cannot capture the changing heat transfer characteristics of PTR with increasing operating temperature, such as the emerged overlapping band window mentioned in Figure 1, and thus hardly meet the demand of high calculation precision for the PTR at high temperature.

In this study, under the assumptions of an even absorber temperature in circumferential and no convection or conduction heat transfers existing in vacuum annular, we establish spectral thermal resistance network

models (Holman, 2001) for accurately simulating the heat loss of PTR and PTR-RS as exhibited in Figure 4(a) and 4(b). In the spectral resistance networks, all parameters employ spectral values per wavelength, namely, spectral absorptance (emittance) of SSC ($\alpha_{\lambda,s}$, $\varepsilon_{\lambda,s}$), spectral transmittance and absorptance of glass envelope ($\tau_{\lambda,\,g}$, $\alpha_{\lambda,\,g}$), spectral emittances of inner and outer surfaces of glass envelope ($\varepsilon_{\lambda,\,k,\,inner}$, $\varepsilon_{\lambda,\,k,outer}$). In the framework of determined absorber temperature (T_s), sky temperature (T_{sky}), and ambient temperature (T_g), the glass envelope temperature (T_g) and radiation shield temperature (T_k) can be obtained by iterative computations. Thus, the spectral thermal resistances (R_λ), radiosities (J_λ), and Blackbody's emissive powers (E_λ) can be calculated out, and then the net spectral heat flux per branch in network ($Q_{r,\,\lambda}$) can be achieved. The total heat fluxes are obtained by accumulating each spectral heat flux at the wavelength from 0.30 μm to 100.20 μm with interval of 0.01 μm. The calculation expressions of spectral thermal resistances and total heat fluxes of PTR and PTR-RS are presented in Table 3.

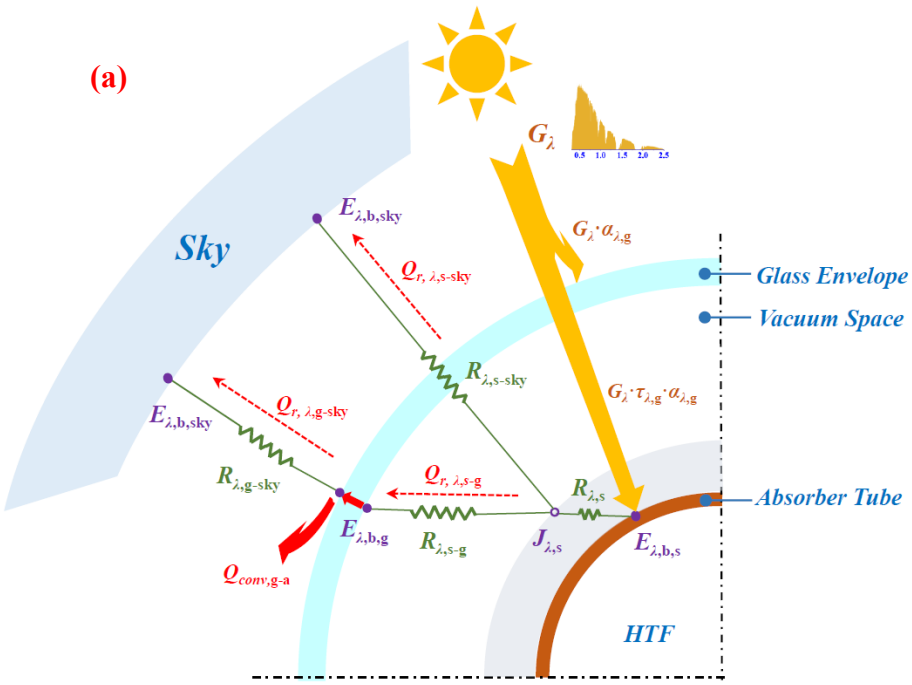

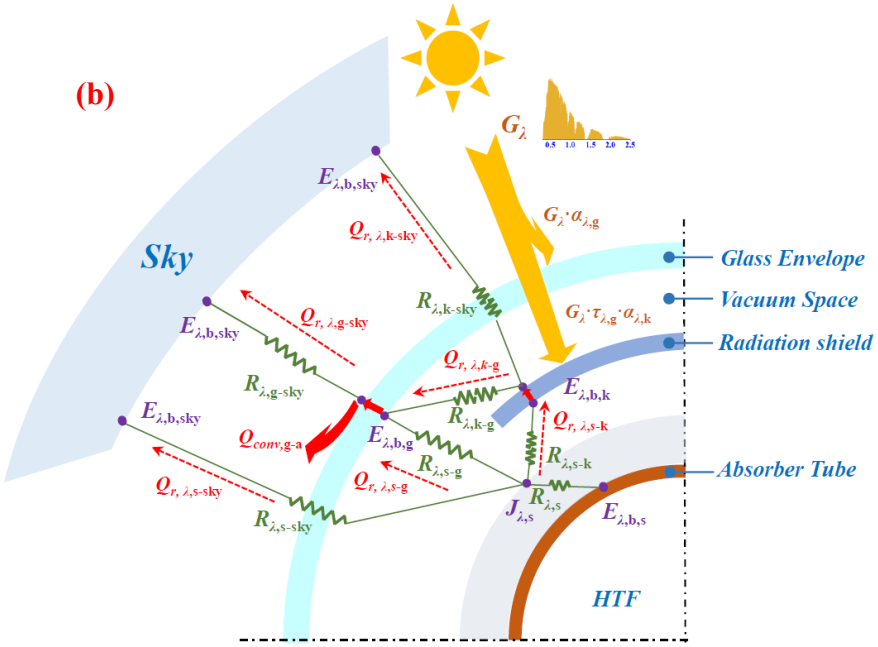

Figure 4. Spectral thermal resistance network in (a) PTR, and (b) PTR-RS. All parameters such as absorptance, emittance, etc. used in network employ spectral values per wavelength. The calculation accuracy of heat loss of PTR is effectively enhanced.

Table 3. Values of spectral thermal resistances and total heat fluxes in PTR and PTR-RS

Spectral thermal resistance	Expression	Heat flux	Expression
$R_{\lambda,\mathrm{s}}$	$1/[A_{\mathrm{s}}^{'}\varepsilon_{\lambda,\mathrm{s}})]$	$Q_{r,\mathrm{s\text{-}sky}}$	$\sum_{\lambda=0.30}^{100.20}\frac{J_{\lambda,\mathrm{s}}-E_{\lambda,\mathrm{b,sky}}}{R_{\lambda,\mathrm{s\text{-}sky}}}\times 0.01$
$R_{\lambda,\mathrm{s\text{-}g}}$	$1/[A_{\mathrm{s}}^{'}F_{\mathrm{s\text{-}g}}(1-\tau_{\lambda,\mathrm{g}})]$	$Q_{r,\mathrm{s\text{-}g}}$	$\sum_{\lambda=0.30}^{100.20}\frac{J_{\lambda,\mathrm{s}}-E_{\lambda,\mathrm{b,g}}}{R_{\lambda,\mathrm{s\text{-}g}}}\times 0.01$
$R_{\lambda,\mathrm{s\text{-}sky}}$	$1/(A_{\mathrm{s}}^{'}F_{\mathrm{s\text{-}sky}}\tau_{\lambda,\mathrm{g}})$	$Q_{r,\mathrm{g\text{-}sky}}$	$\sum_{\lambda=0.30}^{100.20}\frac{E_{\lambda,\mathrm{b,g}}-E_{\lambda,\mathrm{b,sky}}}{R_{\lambda,\mathrm{g\text{-}sky}}+R_{\lambda,g}}\times 0.01$
$R_{\lambda,\mathrm{g\text{-}sky}}$	$1/(A_{\mathrm{s}}^{'}F_{\mathrm{g\text{-}sky}}\varepsilon_{\lambda,\mathrm{g}})$	$Q_{r,k\text{-}\mathrm{g}}$	$\sum_{\lambda=0.30}^{100.20}\frac{E_{\lambda,\mathrm{b,k}}-E_{\lambda,\mathrm{b,g}}}{R_{\lambda,\mathrm{k\text{-}g}}}\times 0.01$
$R_{\lambda,\mathrm{s\text{-}k}}$	$1/(A_{\mathrm{s}}^{'}F_{\mathrm{s\text{-}k}}\varepsilon_{\lambda,\mathrm{k,inner}})$	$Q_{r,\mathrm{k\text{-}sky}}$	$\sum_{\lambda=0.30}^{100.20}\frac{E_{\lambda,\mathrm{b,k}}-E_{\lambda,\mathrm{b,sky}}}{R_{\lambda,\mathrm{k\text{-}sky}}}\times 0.01$
$R_{\lambda,\mathrm{k\text{-}sky}}$	$1/(A_{\mathrm{k}}^{'}F_{\mathrm{k\text{-}sky}}\varepsilon_{\lambda,\mathrm{k,outer}}\tau_{\lambda,\mathrm{g}})$	$Q_{r,\mathrm{s\text{-}k}}$	$\sum_{\lambda=0.30}^{100.20}\frac{J_{\lambda,\mathrm{s}}-E_{\lambda,\mathrm{b,k}}}{R_{\lambda,\mathrm{s\text{-}k}}}\times 0.01$
$R_{\lambda,\mathrm{k\text{-}g}}$	$1/[A_{\mathrm{k}}^{'}F_{\mathrm{k\text{-}g}}(1-\tau_{\lambda,\mathrm{g}})]$	$Q_{conv,\mathrm{g\text{-}a}}$	$h_{\mathrm{c}}(T_{\mathrm{g}}-T_{\mathrm{a}})A_{\mathrm{g}}^{'}$

Noted: *r*, *conv*, and *b* in Figure 4 and Table 3 represent *radiated*, *convective*, and *blackbody's*, respectively. Besides, $A^{'}$ is unit area, m; F is view factor; Q is net heat flux, W/m.

As a result, the total heat loss of PTR and PTR-RS can be expressed as:

$$HL_{PTR} = Q_{r,\text{g-sky}} + Q_{r,\text{s-sky}} + Q_{conv,\text{g-a}}\,, \tag{6}$$

$$HL_{PTR-RS} = Q_{r,\text{g-sky}} + Q_{r,\text{s-sky}} + Q_{r,\text{k-sky}} + Q_{conv,\text{g-a}}\,. \tag{7}$$

3.3.2 Heat-collecting process model

To accurately achieve the heat-collecting characteristics of PTR in real condition, we establish a heat-collecting process model in which all tested PTRs are divided into *n* control volumes. In *no. i* control volume (*i=1, 2, ..., j; j=24*), the heat fluxes, namely, $Q_{r,\text{s-g},i}$, $Q_{r,\text{s-sky},i}$, $Q_{r,\text{g-sky},i}$, and $Q_{conv,\text{g-a},i}$ can be figured out according to the heat loss model in section 3.3.1. Besides, the internal heat transfer between the absorber tube and flowing HTF is expressed as (Padilla et al., 2011):

$$Q_{conv,s-f,i} = h_f A'_{s,i}(T_{s,i} - T_{f,i})\,, \tag{7}$$

where $Q_{conv,s-f,i}$ represents the heat obtained by the HTF from absorber tube in control volume *i*, W/m; h_f is heat transfer coefficient, W/(m^2 • K); $T_{s,i}$ and $T_{f,i}$ are the absorber temperature and HTF temperature in control volume *i*, *K*; $A'_{s,i}$ is unit area of absorber tube in control volume *i*, m.

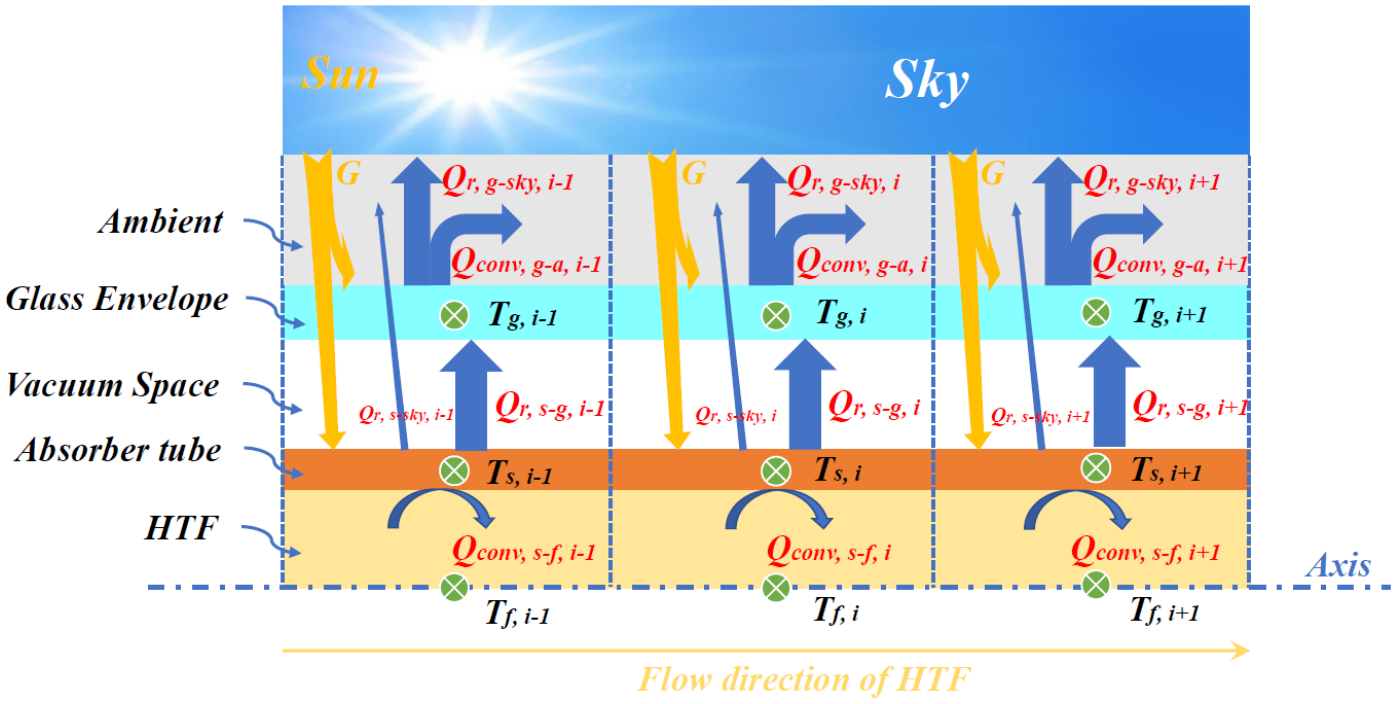

Figure 5. Heat-collecting process model for PTR based on control volume method. The PTR in PTC testing module is divided into a finite number of coupling units (*j*), the heat transfer process and heat gain process in PTR can be preciously calculated and

observed.

The total useful energy obtained by tested PTR in PTC module is

$$Q_{conv,s-f} = L_{volume,i}\sum_{i=1}^{j} Q_{conv,s-f,i}\ ,\ (j=24) \tag{8}$$

where $L_{volume,i}$ is the length of control volume *i*, m; its value is about 0.51 m in this study. As a result, the heat-collecting efficiency of tested PTC module is calculated by

$$\eta = \frac{Q_{conv,s-f}}{A_{ap}G}, \tag{9}$$

where A_{ap} is aperture area of tested PTC module, which is 69 m^2 in this study. G is direct normal solar irradiance, W/m^2.

3.3.3 Exergetic efficiency model

Exergy performance is an important metric used to evaluate the quality in a heat collection process. For a PTC system, the exergy (*EX*) of solar irradiation, according to the most accepted model introduced by Petela [36], is modified as Equation (10). The equivalent solar temperature (T_{solar}) can be set as equal to 5800 K.

$$EX_{solar} = A_{ap}G\bullet[1-\frac{4T_a}{3T_{solar}}+\frac{1}{3}\bullet(\frac{T_a}{T_{solar}})^4]. \tag{10}$$

In the study, the exergy output of the PTC system is equal to the difference of the useful energy and the irreversibility of thermal loss in the nonideal heat transfer process, it can be calculated by the equation as follows:

$$EX_{gain} = Q_{conv,s-f} - m\bullet c_p\bullet T_a\bullet\ln[\frac{T_{ou}}{T_{in}}], \tag{11}$$

where *m* and c_p represent the mass flow rate and the specific heat, respectively, kg/s, J/(kg·K). As a result, the exergy efficiency η_{ex} of PTC system is the ratio of the exergy output EX_{gain} to the exergy of solar irradiation EX_{solar}, i.e.,

$$\eta_{ex} = \frac{EX_{gain}}{EX_{solar}}. \quad (12)$$

4. Results and discussion

4.1 Indoor heat loss

Indoor heat loss results by experiment and simulation are depicted in Figure 6. The experimental heat loss scatter points of PTR and PTR-RS are distributed at absorber temperature approximately from 200 to 540 °C, and they are fitted to well-satisfied heat loss curves which are fourth power functions of absorber temperature in °C (T_s, °C) as presented in Figure 6(a). In the tested absorber temperature, obviously, heat losses of PTR-RS have been consistently lower than these of PTR (Figure 6(a)). And the heat loss reduced by PTR-RS compared with PTR trends to be higher with the increasing absorber temperature, since the RS intercepts much more emissive heat loss from absorber tube which explosively increases with elevating absorber temperature as proved by the fitting heat loss curve. For observing heat loss characteristics of PTR-RS at higher absorber temperature, the simulations are conducted based on established spectral thermal radiation model with high precision. The root-mean-square deviation (*RSME*) (Wang et al., 2019) is used to validate the consistence between the experimental data and numerical results, which is expressed as:

$$RMSD = \sqrt{\frac{\sum[(X_{sim,i} - X_{exp,i}) / X_{exp,i}]^2}{n}}, \quad (13)$$

where $X_{sim,i}$ and $X_{exp,i}$ refer to simulated and experimental data, n is number of data. The comparison results *RMSD* remains within 6.0 %, yielding a satisfactory consistency and thus accurately predicting high-temperature thermal performance of PTR-RS. As depicted in Figure 6(b) combining experimental and simulated values, the relative percentages of heat loss reduced by PTR-RS compared with PTR gradually grow with increasing absorber temperature, the percentage values reach about 26.9% and 28.1% at the experimental and numerical absorber temperatures of 500 and 600 °C. All of heat loss results demonstrate RS exerts a

significantly effective role in reducing heat loss, accordingly, PTR-RS achieves superior thermal performance of heat loss.

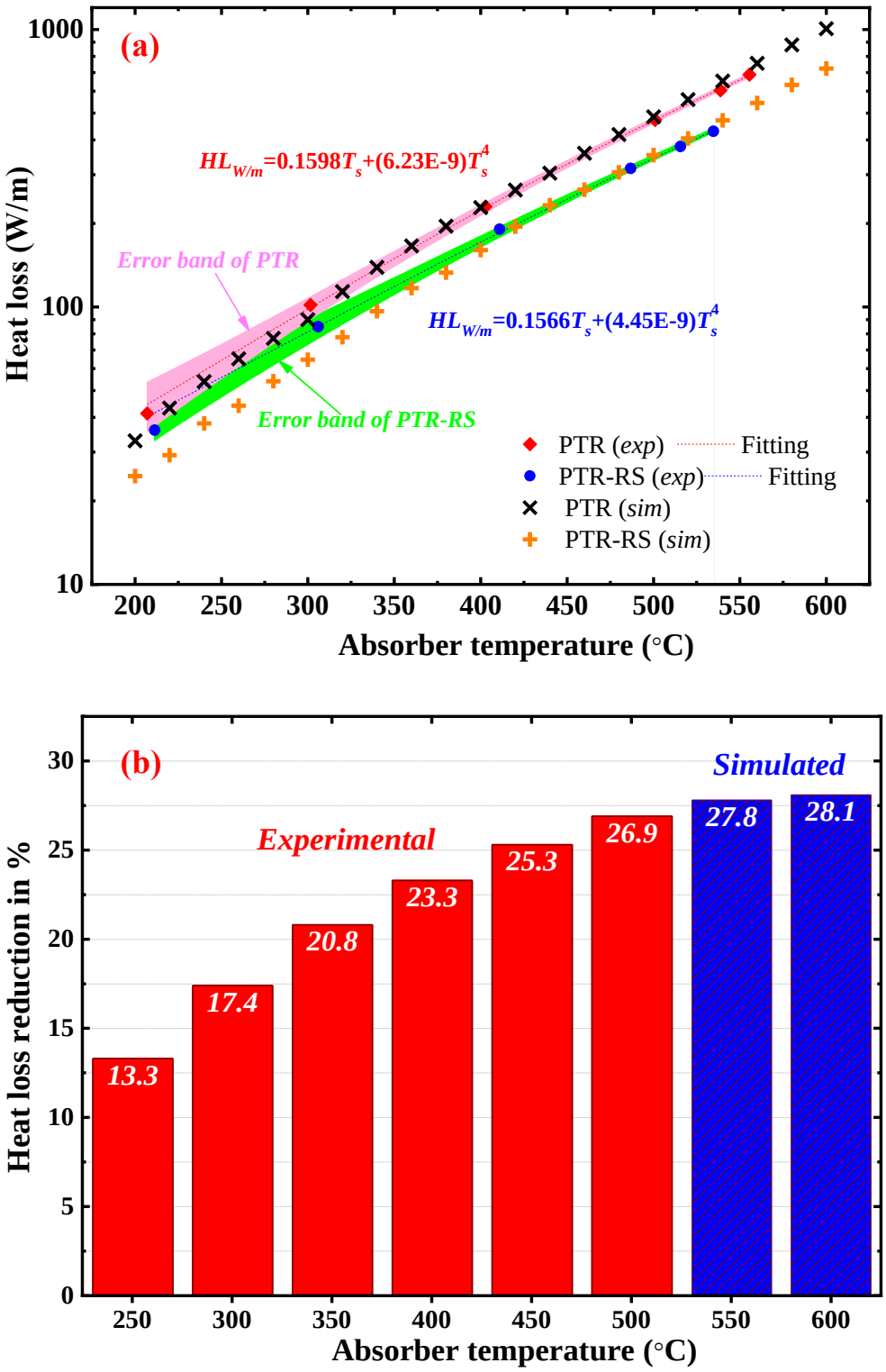

Figure 6. Comparison of emissive heat loss results of PTR and PTR-RS. (a) Experimental and numerical emissive heat loss.

The results validated good effectiveness of RS in PTR-RS to reduce heat loss, and convincing prediction ability of models

especially at high absorber temperature. (b) Relative reduction percentage of heat loss in PTR-RS compared with PTR.

4.2 Outdoor heat-collecting efficiency in experiments and simulations

Proposal of RS according to NTR discovered, as mentioned above, is accessible to make an efficient blockage of heat loss of PTR-RS, but the comprehensive heat-collecting performance of PTR-RS needs to be validated because of incurred solar irradiance loss by RS. Thus, the outdoor heat-collecting efficiency experiments were carried out in a standard two-axis tracking testing platform. The inlet temperatures of HTF of silicone oil were initially set as 250~360 °C for the tested PTRs and PTR-RSs, and their heat-collecting performances were measured under different solar irradiances (G) from 500 to 1000 W/m^2. In the case of average solar irradiance of 780 W/m^2 within fluctuation of ± 80W/m^2, and average ambient temperature of approximately 24°C, to investigate heat-collecting efficiency of PTR and PTR-RS, normalized temperature difference of $\frac{T_f - T_a}{G^{0.5}}$ was employed to process experimental and numerical results as depicted in Figure 7, where T_{in} represents the inlet temperature of PTC testing platform. The heat-collecting efficiency fitting curves used functional relation of $\eta = \eta_0 - Ax - Bx^2, (x = \frac{T_f - T_a}{G^{0.5}})$, where η and η_0 represent the heat-collecting efficiency and optical efficiency of PTC testing platform, A and B are coefficients responding to the linear item and quadratic item. Both values of R-squared (R^2) in PTR and PTR-RS exceed 0.92, which demonstrated the fitting curves matched well with the experimental scatter points of PTR and PTR-RS.

The experimental results and fitting curves show PTR achieved higher heat-collecting efficiency compared with PTR-RS at lower value of normalized temperature difference. Intercept heat-collecting efficiencies at zero-reduced temperature of PTR and PTR-RS are 82.52% and 79.58%, the former is obviously higher than the latter, which can be explained by the existence of RS in PTR-RS. RS in PTR-RS intercepts the incident solar irradiance which should have been projected onto absorber tube in NTR, resulting in the reduced optical

efficiency of PTR-RS at zero-reduced temperature. But the negative effect of RS on the heat-collecting efficiency of PTR-RS abates gradually with the increasing normalized temperature difference. Higher reduced temperature means higher operating temperature of PTR-RS, with which considerable emissive heat loss occurs and RS gradually exerts positive role in reducing the heat loss, causing less emissive heat loss of PTR-RS compared with PTR at the same normalized temperature difference. Therefore, the comprehensive heat loss coefficient of PTR-RS is lower than that of PTR, which can be verified by the descent rate of both efficiency curves in Figure 7. But it has to say that the reduced heat loss is still inferior to make up for the incurred solar irradiance loss by RS until the reduced temperature reaches 9.9 at which the two efficiency curves intersect. Inverse relationship of higher heat-collecting efficiency of PTR compared with PTR-RS occurred at the reduced temperature exceeding 9.9, it is of explainable for this phenomenon that the reduced heat loss by RS increases with the higher operating temperature and make up for the solar irradiance loss at the reduced temperature of 9.9. Accordingly, net heat gain in NTR of PTR-RS is enhanced compared with that of PTR, as a result, PTR-RS achieves superior heat-collecting performance at higher normalized temperature difference. Corresponding to abscissa value of 9.9, average fluid temperature (T_f) and inlet temperature (T_{in}) can be calculated as approximately 304 °C and 300 °C under an assumption of solar irradiance of 800 W/m^2 and ambient temperature of 24 °C.

Simulations based on the real experimental parameters were also carried out and the results depicted in Figure 7 show a satisfactory consistency to the experimental data within 4.5% *RSMD*. This demonstrates that the mathematical model is qualified for performance prediction of PTR and PTR-RS at higher operating temperature which the experiments cannot reach.

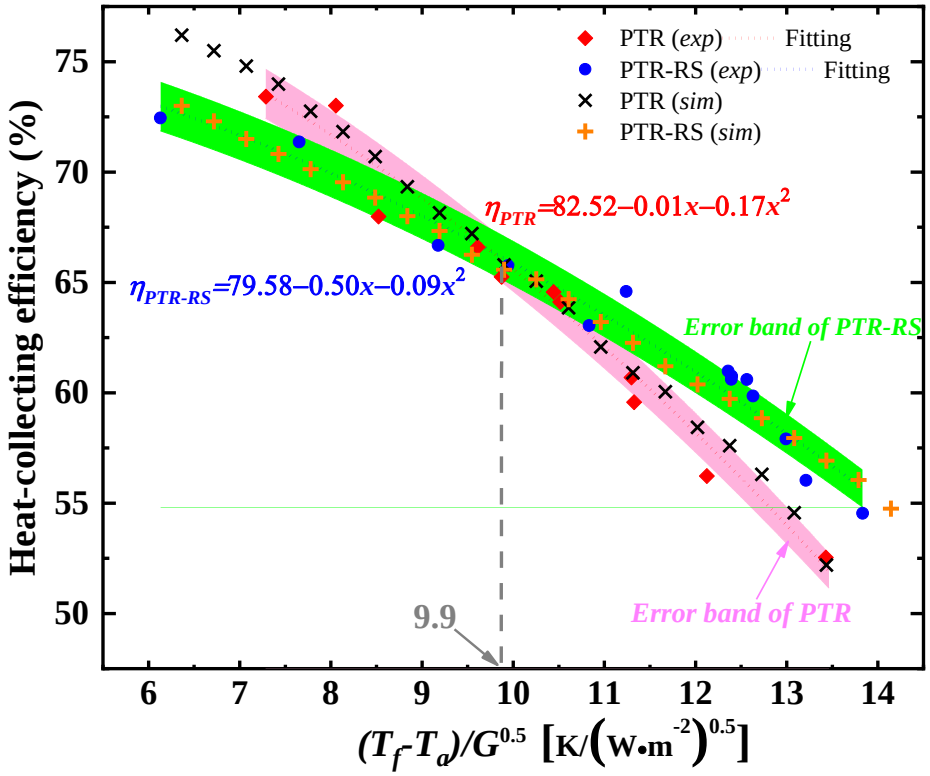

Figure 7. Experimental and numerical heat-collecting efficiency results of PTR and PTR-RS. All of experimental scatter points were measured under average direct solar irradiance of 780 W/m^2 within a fluctuation of ± 80 W/m^2, ambient temperature of approximately 24°C.

4.3 Potential boost of thermal and exergy performance of PTR-RS

Based on the validated models proposed in the study, the simulated inlet temperature of PTC testing platform was extended to 400~550 °C by using molten salt as HTF to observe the potential performance boost of the PTR-RS. As shown in Figure 8 and Figure 9, the heat-collecting efficiency and exergetic efficiency of the PTR and PTR-RS are calculated and exhibited in the cases of different solar irradiances and inlet temperatures. The experimental and numerical results at the inlet temperature of 300~350 °C and 400~550 °C show that higher operating temperature and lower solar irradiance contribute larger enhancements of heat-collecting efficiency and exergetic efficiency of PTR-RS compared with PTR. Therefore, the largest enhancement percentages occur at the solar irradiance of 600 W/m^2 and inlet temperature of 550 °C, where the values of heat-collecting efficiency and exergetic efficiency of the PTR and PTR-RS reach 49.1 and 30.7 %,

55.4 and 36.1 %, the heat-efficiency and exergetic efficiency of PTR-RS are relatively enhanced by 12.9 and 17.6 % compared with the PTR. The detailed relative percentages of performance enhancement in comparisons between the PTR-RS and PTR are presented in Table 4.

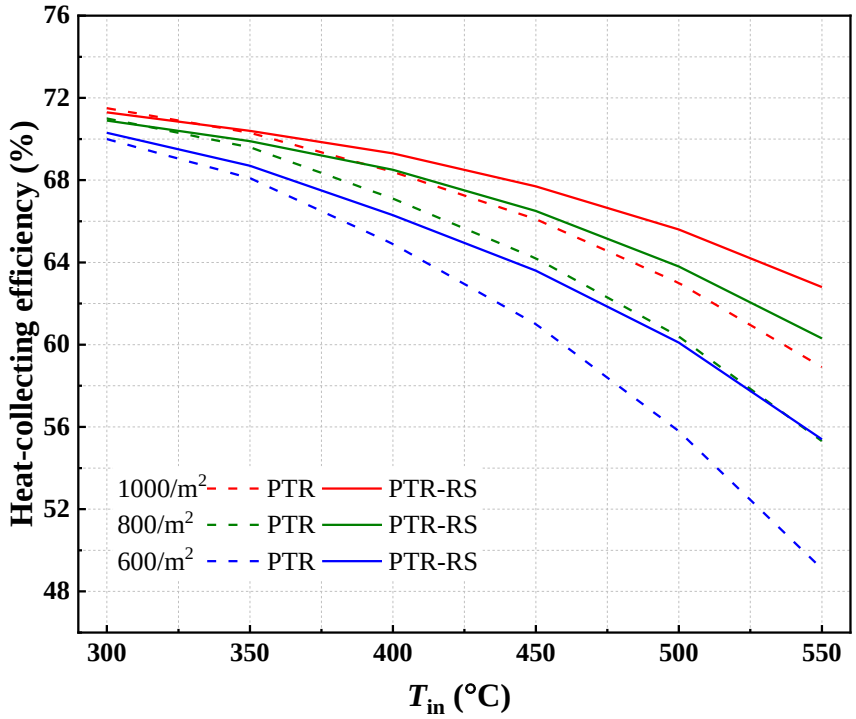

Figure 8. Heat-collecting efficiencies of PTR and PTR-RS under different solar irradiances and inlet temperatures

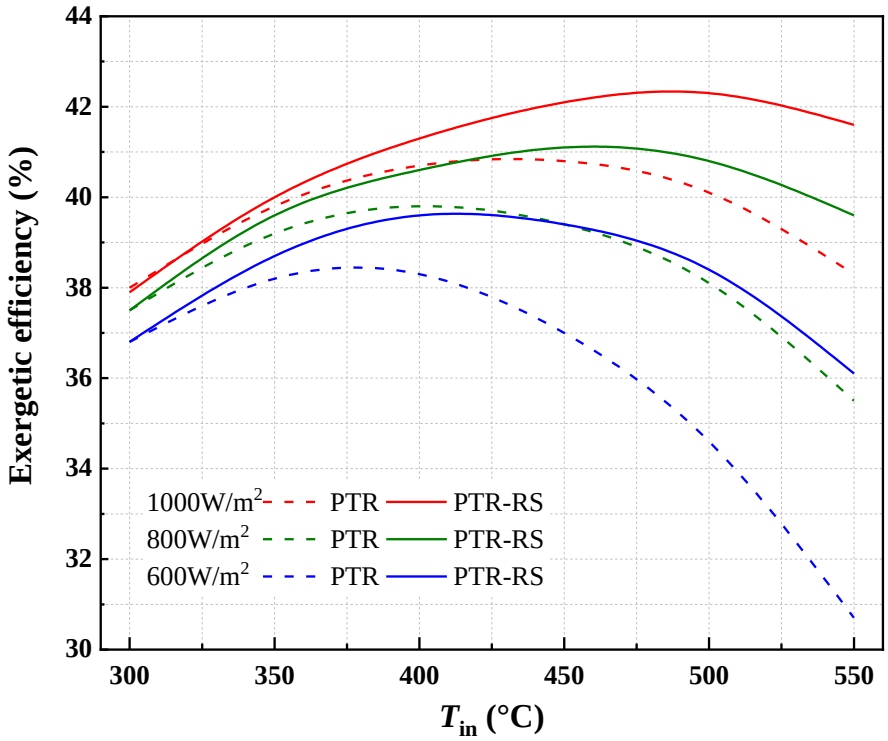

Figure 9. Exergetic efficiencies of PTR and PTR-RS under different solar irradiances and inlet temperatures

Actually, the rules of heat-collecting and exergetic efficiencies of PTR-RS related to operating temperature and solar irradiance coincide with our conjecture about the RS in the NTR, lower solar irradiance causes less solar irradiance loss incurred by RS and higher operating temperature promotes the role of RS in reducing emissive heat loss, originally, enhancing the net heat gain in NTR of PTR. In the case of inlet temperature of 300 °C and solar irradiance of 1000 W/m^2, as presented in Table 4, the relative percentages of the enhanced heat-collecting efficiency and exergetic efficiency are -0.3, which demonstrate the net heat gain is reduced in PTR-RS in comparison to PTR at such high solar irradiance and low operating temperature. Positive role of RS in enhancement of net heat gain in PTR-RS thus the heat-collecting and exergetic efficiencies are exerted with higher operating temperature and lower solar irradiance.

Table 4. Relative percentages of the enhancements of heat-collecting and exergetic efficiencies ($RP_{thermal}$, $RP_{exergetic}$)of PTR-RS compared with PTR

T_{in}	1000 W/m^2		800 W/m^2		600 W/m^2	
	$RP_{thermal}$ (%)	$RP_{exergetic}$ (%)	$RP_{thermal}$ (%)	$RP_{exergetic}$ (%)	$RP_{thermal}$ (%)	$RP_{exergetic}$ (%)
300 °C	**-0.3**	**-0.3**	**0.0**	**0.0**	**0.5**	**0.3**
350 °C	**0.1**	**0.5**	**0.5**	**1.0**	**0.8**	**1.3**
400 °C	**1.3**	**1.5**	**2.0**	**2.0**	**2.2**	**3.4**
450 °C	**2.5**	**3.2**	**3.5**	**4.3**	**4.3**	**6.5**
500 °C	**4.1**	**5.5**	**5.7**	**7.1**	**7.6**	**11.0**
550 °C	**6.5**	**8.6**	**9.1**	**11.5**	**12.9**	**17.6**

4.4 Role of NTR improvement in performance enhancement of PTR-RS

Undoubtedly, the addition of RS plays an effective role in enhancing the photothermal conversion efficiency of PTR-RS, the original reason for that is improvement of heat transfer characteristic and net heat gain of NTR

in PTR-RS. The absorbed solar irradiance and emissive heat loss were calculated and depicted in Figure 10. In the case of absorber temperature of 600 °C and solar irradiance of 600 W/m^2, it is noted that the value of γ_{emi} of PTR in NTR remarkably decreases compared with that of PTR-RS in NTR, and the net heat gains of PTR and PTR-RS in NTR are -5.95π and -1.64π rad, the latter with RS is relatively reduced by 72.4% compared with the former. The effective reduction of emissive heat loss contributes to not only the high reflectance of inner surface of RS but also SSC covered on the outer surface of RS, which make RS absorb the solar irradiance and obtain high temperature of 464 °C, further decreasing the heat transfer between the absorber tube and RS.

Additionally, the total net heat gains of PTR and PTR-RS by accumulating net heat gain values of NTR and non-NTR are 33.67π and 37.98π rad, a relative enhancement of net heat gain (heat-collecting efficiency) by 12.8% is achieved by the PTR-RS compared with PTR. The validity of this relative percentage enhancement of heat-collecting efficiency could be proved by value of 12.9 % in Table 4. In the case of inlet temperature of 550 °C and solar irradiance of 600 W/m^2, the average operating temperature of fluid in PTC testing platform is 552.5 °C, and the corresponding average absorber temperature approximately reaches 600 °C with a consideration of temperature difference of almost 40~50 °C between the fluid temperature and absorber temperature.

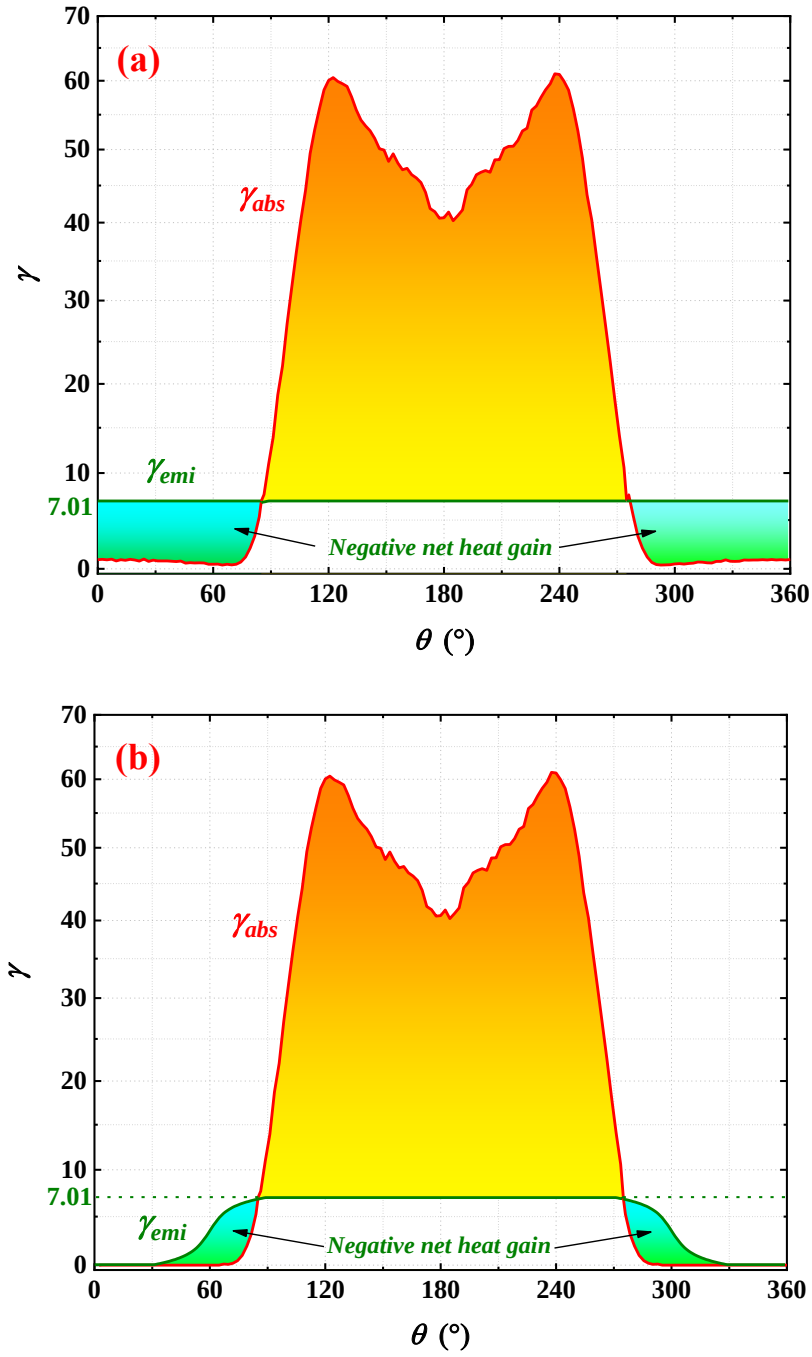

Figure 10. Net heat gain in (a) PTR and (b) PTR-RS. In the case of absorber temperature of 600 °C and direct solar irradiance of 600 W/m^2, the net heat gain of PTR-RS in NTR is effectively improved by 72.4% compared with that of PTR. RS would be more influential to reduce the heat loss in NTR and improve net heat gain of PTR-RS in lower solar irradiance and higher absorber temperature.

Actually, the NTR in PTR-RS could be further optimized since negative net heat gain still occurs though most has been eliminated compared with PTR. Besides of further optimization of structure and parameters on

the introduced RS, the other three optimization methods or their compound optimization methods to the NTR mentioned above would work, this part of research would be investigated in the next step. Without doubt, this research on the new PTR-RS based on the scientific definition of NTR proposes a new approach to effectively enhance the thermal performance of PTR.

5. Conclusion

The study discovers and proposes a negative thermal-flux region (NTR) in parabolic trough receiver (PTR). Based on the heat transfer characteristic of NTR, optimization methods to reinforce the reduction of heat loss in NTR rather than persistent enhancement of solar irradiance absorption like previous studies are put forward for elevating the photothermal conversion performance of PTR. Besides, we investigate the role played by radiation shield inserted into the vacuum annular of PTR in NTR in the reduction of heat loss and enhancement of heat-collecting efficiency of PTR. Accordingly, the present study demonstrates PTR with RS (PTR-RS) has a great potential to possess breakthrough enhancement of photothermal conversion performance at high operating temperature, which is entirely feasible in practical engineering. The other optimization methods proposed would be more efficient and effective and they will be investigated in the next step.

In this study, compared with the prototype PTR, the heat loss of proposed PTR-RS is effectively reduced by 28.1% at absorber temperature of 600 °C, the heat-collecting efficiency and exergetic efficiency are significantly enhanced by 12.9 and 17.6 % at the solar irradiance of 600 W/m^2 and inlet HTF temperature of 550 °C. Superior performance of PTR-RS would be obtained under the lower solar irradiance and higher operating temperature.

Based on the proposed theory of negative thermal-flux region (NTR), in the future research, the techno-economic feasibility of the PTR-RS in a real CSP plant will be investigated. It's worth mentioning that, though the actual cost of PTR-RS studied in this paper increases by 5 %, annual net electricity production is predicted

to increase by 5-10% compared with the conventional PTR, which is a huge boost for the CSP and cleaner production field of concentrated solar energy. Furthermore, the feasibility analyses on the other optimization methods proposed in section 3 will be also carried out. For instance, covering IR-reflector coatings with adjustable cutoff wavelength caused by temperature or electricity on the inner and outer surfaces of the glass envelope in the NTR to adaptively intercept the emissive heat loss as well as let a certain amount of solar irradiance pass through. Predictably, these optimization methods will make promising contributions to effectively reduce the radiation heat loss and thus enhance the overall thermal performance of the PTR.

Competing interests

The authors declare no competing financial interest.

Acknowledgement

This study was sponsored by National Science Foundation of China (51761145109, 51776193), the ITF Postdoctoral Hub programme of The Hong Kong SAR Government, China, and China Postdoctoral Science Foundation (2019M652209).

References

Al-Soud, M. S., Hrayshat, E. S., 2009. A 50 MW concentrating solar power plant for Jordan. Journal of Cleaner Production, 17(6), 625-635.

Bellos, E., Tzivanidis, C., 2019. Alternative designs of parabolic trough solar collectors. Progress in Energy and Combustion Science, 71, 81-117.

Bellos, E., Tzivanidis, C., 2020. Enhancing the performance of a parabolic trough collector with combined

thermal and optical techniques. Applied Thermal Engineering, 164, 114496.

Benidir, A., Fouad, K., Hakim, B. A., Fethi, B., 2018. Numerical Thermal Analysis of Schott 2008 PTR70 Solar Receiver Under Hassi R'mel Power Plant Operation Conditions. Journal of Engineering Science and Technology, 13(1), 122-140.

Burkholder, F., Kutscher, C., 2009. Heat loss testing of Schott's 2008 PTR70 parabolic trough receiver (No. NREL/TP-550-45633). National Renewable Energy Lab.(NREL), Golden, CO (United States).

Cespedes, E., Wirz, M., Sánchez-García, J. A., Alvarez-Fraga, L., Escobar-Galindo, R., Prieto, C., 2014. Novel Mo–Si3N4 based selective coating for high temperature concentrating solar power applications. Solar energy materials and solar cells, 122, 217-225.

Chen, Q. F., Yuan, Z. X., Guo, Z. Q., Zhao, Y., 2019. Practical performance of a small PTC solar heating system in winter. Solar Energy, 179, 119-127.

Cheng, Z. D., He, Y. L., Cui, F. Q., 2012. Numerical study of heat transfer enhancement by unilateral longitudinal vortex generators inside parabolic trough solar receivers. International journal of heat and mass transfer, 55(21-22), 5631-5641.

Duffie J A, Beckman W A, Blair N., 2020. Solar Engineering of Thermal Processes, Photovoltaics and Wind. John Wiley & Sons.

Dugaria, S., Bortolato, M., Del Col, D., 2018. Modelling of a direct absorption solar receiver using carbon based nanofluids under concentrated solar radiation. Renewable Energy, 128, 495-508.

Feldhoff, J. F., Schmitz, K., Eck, M., Schnatbaum-Laumann, L., Laing, D., Ortiz-Vives, F., Schulte-Fischedick, J., 2012. Comparative system analysis of direct steam generation and synthetic oil parabolic trough power plants with integrated thermal storage. Solar Energy, 86(1), 520-530.

Fernández-García, A., Rojas, E., Pérez, M., Silva, R., Hernández-Escobedo, Q., Manzano-Agugliaro, F.,

2015. A parabolic-trough collector for cleaner industrial process heat. Journal of Cleaner Production, 89, 272-285.

Fuqiang, W., Ziming, C., Jianyu, T., Yuan, Y., Yong, S., Linhua, Lx. Progress in concentrated solar power technology with parabolic trough collector system: A comprehensive review. Renewable and Sustainable Energy Reviews 2017, 79, 1314-1328.

He, Y. L., Qiu, Y., Wang, K., Yuan, F., Wang, W. Q., Li, M. J., Guo, J. Q., 2020. Perspective of concentrating solar power. Energy, 117373.

Holman J P., 2001. Heat transfer, eighth SI metric edition. Mc Gran–Hill Book Company.

Incropera, F. P., Lavine, A. S., Bergman, T. L., DeWitt, D. P., 2007. Fundamentals of heat and mass transfer. Wiley.

Jaramillo, O. A., Borunda, M., Velazquez-Lucho, K. M., Robles, M., 2016. Parabolic trough solar collector for low enthalpy processes: An analysis of the efficiency enhancement by using twisted tape inserts. Renewable energy, 93, 125-141.

Kalogirou S A. A detailed thermal model of a parabolic trough collector receiver. Energy 2012, 48(1): 298-306.

Khan, J., Arsalan, M. H., 2016. Solar power technologies for sustainable electricity generation–A review. Renewable and Sustainable Energy Reviews, 55, 414-425.

Koroneos, C., Tsarouhis, M., 2012. Exergy analysis and life cycle assessment of solar heating and cooling systems in the building environment. Journal of Cleaner Production, 32, 52-60.

Kutscher C, Burkholder F, Kathleen Stynes J., 2012. Generation of a parabolic trough collector efficiency curve from separate measurements of outdoor optical efficiency and indoor receiver heat loss. Journal of solar energy engineering, 134(1).

Li G., 2019. Design and development of a lens-walled compound parabolic concentrator-a review. Journal of Thermal Science, 28(1), 17-29.

Li, G., Xuan, Q., 2020. Akram M W, et al. Building integrated solar concentrating systems: A review. Applied Energy, 260, 114288.

Li, Q., Zhang, Y., Wen, Z. X., Qiu, Y., 2020. An evacuated receiver partially insulated by a solar transparent aerogel for parabolic trough collector. Energy Conversion and Management, 214, 112911.

López-Herraiz, M., Fernández, A. B., Martinez, N., Gallas, M., 2017. Effect of the optical properties of the coating of a concentrated solar power central receiver on its thermal efficiency. Solar Energy Materials and Solar Cells, 159, 66-72.

Maccari, A., Bissi, D., Casubolo, G., Guerrini, F., Lucatello, L., Luna, G., ... Zuanella, M., 2015. Archimede Solar Energy molten salt parabolic trough demo plant: a step ahead towards the new frontiers of CSP. Energy Procedia, 69, 1643-1651.

Mahlangu, N., Thopil, G. A., 2018. Life cycle analysis of external costs of a parabolic trough Concentrated Solar Power plant. Journal of Cleaner Production, 195, 32-43.

Padilla R V, Demirkaya G, Goswami D Y, et al. Heat transfer analysis of parabolic trough solar receiver. Applied Energy 2011; 88(12): 5097-110.

Pitz-Paal, R., 2017. Concentrating solar power: still small but learning fast. Nature Energy, 2, 17095.

Soum-Glaude, A., Le Gal, A., Bichotte, M., Escape, C., Dubost, L., 2017. Optical characterization of TiAlNx/TiAlNy/Al2O3 tandem solar selective absorber coatings. Solar Energy Materials and Solar Cells, 170, 254-262.

Singh, N., Khullar, V., 2019. Efficient Volumetric Absorption Solar Thermal Platforms Employing Thermally Stable-Solar Selective Nanofluids Engineered from Used Engine Oil. Scientific reports, 9(1), 1-12.

Trieb, F., Müller-Steinhagen, H., Kern, J., Scharfe, J., Kabariti, M., Al Taher, A., 2009. Technologies for large scale seawater desalination using concentrated solar radiation. Desalination, 235(1-3), 33-43.

Vignarooban, K., Xu, X., Arvay, A., Hsu, K., Kannan, A. M., 2015. Heat transfer fluids for concentrating solar power systems–a review. Applied Energy, 146, 383-396.

Wang, Q., Li, J., Yang, H., Su, K., Hu, M., & Pei, G. Performance analysis on a high-temperature solar evacuated receiver with an inner radiation shield. Energy 2017, 139, 447-458.

Wang, Q., Hu, M., Yang, H., Cao, J., Li, J., Su, Y., Pei, G., 2019. Performance evaluation and analyses of novel parabolic trough evacuated collector tubes with spectrum-selective glass envelope. Renewable energy, 138, 793-804.

Wang, Q., Hu, M., Yang, H., Cao, J., Li, J., Su, Y., & Pei, G. Energetic and exergetic analyses on structural optimized parabolic trough solar receivers in a concentrated solar–thermal collector system. Energy 2019, 171, 611-623.

Wirz, M., Petit, J., Haselbacher, A., Steinfeld, A., 2014. Potential improvements in the optical and thermal efficiencies of parabolic trough concentrators. Solar Energy, 107, 398-414.

Zhang, H. L., Baeyens, J., Degrève, J., & Cacères, G., 2013. Concentrated solar power plants: Review and design methodology. Renewable and sustainable energy reviews, 22, 466-481.